Volume 17, Number 1, 2024. pp. 45-57

Jordan Journal of Physics

ARTICLE

Beam Dynamics Studies for a Proposed H – type DTL Using in Eye Therapy

Ali M. Almomani[a], **Mohammad H. Maabreh**[a], **Molham M. Eyadeh**[a] and **Suha M. Alzubaidi**[b]

[a] *Physics Department, Faculty of Science, Yarmouk University, Irbid 21163, Jordan.*
[b] *Aydon, Irbid 21166, Jordan.*

Doi: **https://doi.org/10.47011/17.1.5**
Received on: 21/04/2022; *Accepted on: 28/08/2022*

Abstract: In this study, we explore the KONUS (Kombinierte Null Grad Struktur) beam dynamic studies using a 3D–PIC LORASR simulation code for a specialized medical drift tube linac designed for eye therapy. A total acceleration voltage of 70.89 MV is applied through 6 CH–DTL (3 coupled and 3 non-coupled) cavities within a total of 140 gaps, spanning a length of 20 m. This setup is designed to accelerate protons from an initial energy of 3 MeV to 70 MeV, tailored for application in eye therapy. Each cavity operates at a frequency of 325.244 MHz. To maintain transverse matching of the beam, 11 triplet quadrupole lenses are distributed along the linac structure, including one in the transport section. The beam dynamics analysis provides actual values for the lengths of drift tubes and gaps. To ensure linac stability, simulations are conducted to assess machine errors. The obtained lengths of drift tubes, gaps, and periods serve as the foundation for constructing the RF model for each cavity using the CST Studio Suite. The overall results are quite promising, indicating the viability of proceeding to the next phase, which includes RF simulations and mechanical modeling.

Keywords: LORASR code, KONUS, Beam dynamics, DTL, CST, Eye therapy.

1. Introduction

The development of particle accelerators was motivated by experiments in nuclear physics. The concept of using a particle beam to investigate the structure of matter was developed after the Rutherford scattering experiments. On the other hand, the medical accelerators date back to the history of particle accelerators since Roentgen discovered the X-ray tube in 1895 [1]. In comparison with circular accelerators, linacs can provide a proton beam with reduced momentum spread and size. Moreover, linacs have other advantages, including strong focusing in high-intensity machines, the avoidance of repetitive errors, and well-developed capabilities for injection and extraction, enabling operation at any duty factor.

The Alvarez DTL represents the standard solution for the hadron (protons and ions) acceleration. However, the currently used FODO lattice (focusing–drift–defocusing–drift), where the magnetic quadrupole is hosted inside each drift tube, amplifies the mechanical fabrication efforts and poses challenges for RF tuning [2]. As an alternative in the low beta range, H-mode drift tube linacs emerge as a prominent choice. Currently, there are two types of H-mode drift tube linacs the interdigital H-mode DTL (IH-DTL) for a frequency range of 30-200 MHz [2, 3], and the crossbar H-mode DTL (CH–DTL) intended for higher frequencies necessary for achieving energies up to hundred MeV [3]. The H–type cavities (IH– and CH–DTL) have many

Corresponding Author: Ali M. Almomani **Email**: ali.almomani@yu.edu.jo

advantages over conventional Alvarez structures. These include high shunt impedance, leading to reduced operational costs, greater robustness against beam losses, a smaller size, and a simpler mechanical design, which results in lower fabrication costs [2-3]. Figure 1 shows the H–type DTL family.

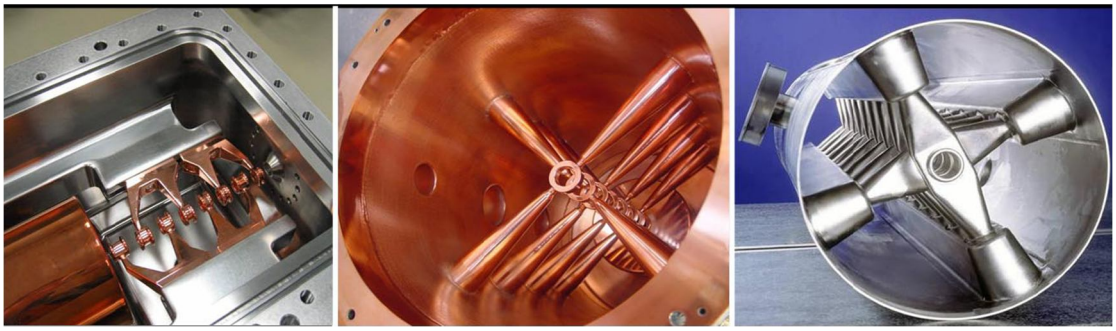

FIG. 1. H-type DTL family [2-3]. The 216.816MHz room temperature IH-DTL for HICAT (left), the 325 MHz room temperature CH-DTL prototype for FAIR (middle) and 325 MHz superconductor CH-DTL prototype (right).

Radiotherapy is one of the most widely used cancer treatments today. The discovery of X-rays and natural radioactivity by Rontgen and Becquerel in the late 19th century was the first step toward radiation treatment [4]. Another significant trend is the use of charged particle radiotherapy, employing proton or carbon ions for specific types of cancers such as ocular melanomas, originating from pigment cells in the eye [5]. It is also used as adjuvant therapy for skull base chondroma, chondrosarcoma, and spine (usually cervical) [4]. There is great pressure on the scientific community to introduce accelerators used for radiotherapy, aiming to provide the best possible methods of treating cancer at the lowest cost.

In spite of the fact that other alternative treatments exist to cure the cancer such as surgery (either resection or total enucleation), chemotherapy, brachytherapy, and thermotherapy, proton treatment options offer advantages due to their ability to spare healthy visual and intracranial tissues. The use of protons for ocular cancer treatment began in 1972, leveraging the precise dose deposition profiles of protons to deliver a high-dose treatment field while preserving healthy tissues and adjacent organs, such as the optic nerve. Several studies demonstrate satisfactory clinical results for ocular cancer patients treated with proton therapy.

When a proton penetrates a material, it interacts with the surrounding media, mainly through Coulomb's interactions with electrons, nuclear reactions, and ionization of particles. Thus, the proton loses energy, depositing it along its path. The dose absorbed in the matter (energy absorbed per unit mass) is proportional to the number of ionization, or the energy transferred per unit length (keV/µm), which is called linear energy transfer (LET) or stopping power.

As the energy of the proton decreases, both the interaction cross section and the stopping power increase. This leads to an increase in energy deposition with depth until the protons eventually come to a stop. The entry dose is relatively low, followed by a rise to the high-dose area and then a sharp drop to zero. In 1903, this phenomenon was observed by physicist William Henry Bragg and is now known as the Bragg peak [6]. In the case of eye treatment, the required proton beam range is limited by the eye size, typically about 2.5 cm [7], corresponding to a proton energy of around 70 MeV. Numerous facilities worldwide, such as IFJ in Krakow [8], UCSF in San Francisco [9], INFN-LNS in Catania [10], CCO in Wirral [11], CAL in Nice [12], HZB-Charite in Berlin [13], TRIUMF in Vancouver [14], and COP in Orsay [15], have been established to treat ocular tumors using proton therapy. The proton energy in these facilities ranges from 58.0 to 75.0 MeV [7].

Although all currently operational or under-construction hadron therapy facilities rely on circular accelerators (synchrotrons or cyclotrons) [16], the linear accelerator shows quite promising advantages that neither the cyclotron nor the synchrotron can provide. For example, the linac can offer a very small transverse emittance that allows for a smaller beam diameter. Moreover, the energy and beam intensity can be quickly varied within a couple of ms in linacs.

Unlike other types of accelerators, a linac does not require the use of complex injection and extraction systems or energy selection systems. This eliminates the need for mechanical devices and passive components, which are typically required for the maintenance and reliability of these systems [16].

The beam emittances of linacs typically range between 1 and 2 π mm·mrad, which is smaller compared to the beam produced by cyclotrons, which can exceed 4 π mm·mrad. This characteristic aids in reducing the beam size, allowing for the generation of a more focused or pencil beam [17].

This paper focuses on beam dynamics studies for a drift tube linac designed to accelerate a proton beam to energies ranging between 58 and 70 MeV. Within this energy range, the proton beam becomes suitable for radiotherapy applications, specifically in the treatment of eye cancer. Higher beam energies are required for addressing deep-seated tumors within the human body.

2. Methodology

2.1 KONUS Beam Dynamics

The use of the KONUS (**KO**mbinierte **NU**ll grad **S**truktur – Combined Zero Degree Structure) beam dynamics allows one to maximize the applied acceleration voltage between two focusing elements (quadrupoles) [18].

The main idea of the KONUS beam dynamics is to apply the 0° synchronous phase in the accelerating gap to maximize the acceleration efficiency, and thus minimize the RF defocusing in transverse planes, allowing the beam to pass many accelerating gaps between two transversely focusing lenses [18]. Another benefit is an increased energy gain in the linac structure by accelerating the beam near a synchronous phase $\varphi_s = 0$, as seen in Fig. 2, which shows the synchronous particle motion at zero synchronous particle phase.

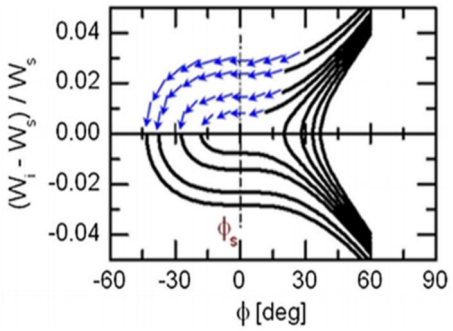

FIG. 2. Schematic plot for particle trajectories in the longitudinal phase space at $\varphi_s = 0$ (KONUS uses only the area marked by blue arrows in the longitudinal phase space).

Fig. 3 shows the KONUS period, which consists of a transverse focusing lens (solenoid or quadrupole triplet), a short negative synchronous particle section for longitudinal matching, and a main acceleration section along a zero synchronous structure. The heart of KONUS consists of the main acceleration sections defined by a 0º synchronous particle. In this section, the bunch center is injected with increased energy relative to the 0º synchronous particle. Because of this extra energy, the bunch center will encounter the next gap when the field is not on the top and with a more negative phase, thus reducing the energy difference with respect to the synchronous particle.

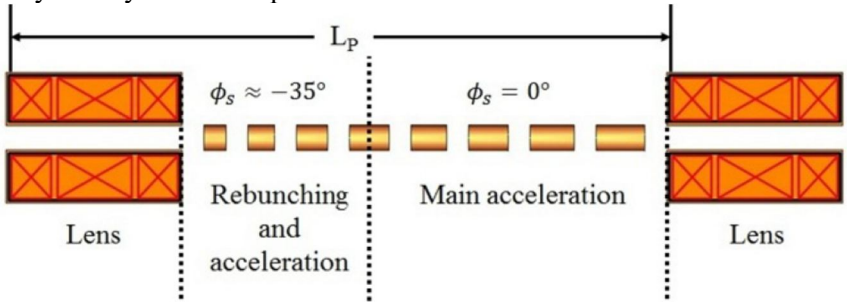

FIG. 3. A scheme of the H-type drift tube linac, showing the separated function principle KONUS – beam dynamics with respect to acceleration and beam focusing.

2.2 LORASR Code

The LORASR code (**Lo**ngitudinal und **ra**diale **S**trahldynamikrecnungen mit **R**aumladung), which means longitudinal and radial beam dynamics simulation, including space charge effect, has been developed at the Institute for Applied Physics, Frankfurt University in collaboration with GSI – Darmstadt. The code is specialized for the beam dynamics design of "Separate Function DTLs" in general and in particular on the "Combined 0-degree structure (KONUS)" beam dynamics [19].

The investigations of beam dynamics are performed using the LORASR code of the structure based on a KONUS. The LORASR code has been used for several years successfully in more than one project around the world, including the Rex-Isolde at CERN [20], the HLI at GSI [21], the carbon injectors in the cancer therapy centers HIT (Germany) [22], and FAIR proton linac [23]. Moreover, KONUS beam dynamics has been used to design the IH – DTL structure for the Korea Heavy Ion Medical Accelerator (KHIMA) project [24], where the $^{12}C^{+4}$ beam was accelerated from an input energy of 0.4 MeV/u to an output energy of 7 MeV/u by the IH-DTL operated at 200 MHz [24].

In the code development process, error handling mechanisms have been implemented to address machine errors and ensure robustness. This includes checking for energy loss profiles and implementing steering correction strategies to optimize performance and accuracy. [18]. The most important causes of these errors during operation are static and dynamic errors such as failure in manufacturing, adjusting components, instability of the RF source, and mechanical vibrations [25]. The manual input is appropriate when data from measurements are available (e.g. quadrupole alignment listings or measured gap voltages).

2.2 Designing Procedure

The key points for any design are purpose and energy. This will draw the broad lines for any design and will define the number of cavities, gaps per cavity, effective applied voltage, structure length, and the beam parameters, including energy and emittances. In this work, the linac for eye proton therapy was designed (up to 70 MeV). Different tumor types will need different energies for example brain tumors will need protons with energies up to 250 MeV.

Typically, the DTL part will be preceded by a Radio-Frequency Quadrupole (RFQ) which can deliver the particles with energy up to 3 MeV and this is the case in our proposed structure. The first cavity behind the RFQ will be the most critical one; because it will be used not only for beam acceleration but also for beam matching. Thus, in our structure, we prefer for the first cavity to have the rebunching section built separated from the cavity itself, which means that we have only the zero section part and the quadrupole from the KONUS lattice. For other cavities, the rebunching section will be a part of them and they will follow the lattice definition as in Fig. 2.

By variation of the starting conditions phase spread ($\Delta\varphi$) and energy spread (ΔW) of the first gap of each 0° section, the desired output parameters (distribution shape and orientation) can be matched to the needs of the following sections.

In principle, the higher the number of gaps in 0^{o} - section the better for efficient acceleration but there are several constraints that must be kept: the longitudinal matching, transverse matching, and well-balanced ratio between the number of gaps in rebunching section and the number of gaps in 0^{o} section which is typically between 1:2 and 1:4, but could be more based on the particle distributions, the maximum number of gaps per section up to 20 gaps and per tank up to 60 gaps. The maximum number of gaps is limited by the tank voltage flatness reasons and the available RF power klystron. The effect of increasing the gaps in 0^{o} section by adding some gaps on the longitudinal motion resulted in rotating the beam distribution and increased the energy spread and on transverse motion where the beam is much more diverged.

Our design was optimized based on the mentioned criteria and as a result, the number of rebunching gaps for each cavity ranged between 3 and 4 gaps while the number of gaps in 0^{o} section was between 8 and 17 gaps. It should be noted that the number of macro particles that were used in simulations is about 10^6 particles.

3. Results and Discussion

3.1 70 MeV Linac Design

The general layout of a DTL part for the proton eye therapy is shown in Fig. 4. Typically, the proton beam is generated in an ion source with a maximum current of about 1 mA (in this study). The subsequent Low Energy Beam Transport (LEBT) provides the required separation of protons, it works as a matching between the ion source and the radio-frequency quadrupole (RFQ). At this point, the beam is bunched and accelerated by an RFQ up to about the energy of 3 MeV (typical range of RFQ). Finally, the main acceleration will be performed by the DTL part, which will be the topic of this work.

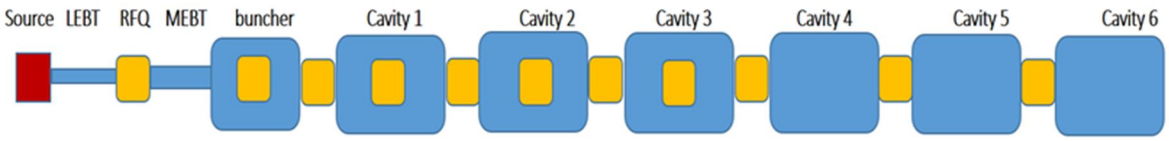

FIG. 4. The layout of the DTL design including the ion source, RFQ and MEBT. The blue boxes represent the cavities, LEBT, MEBT and buncher and the yellow elements are the triplet quadruples magnets. Cavities 1, 2 and 3 are coupled cavities.

In order to match the beam from RFQ into the first cavity by rotating the beam to reduce the phase spread and increase the energy spread, a two-gap rebuncher cavity is added (as shown in Fig. 4). All cavities, including the rebuncher, will be operated at 325.244 MHz that fits with the available amplifier.

In order to reach the required energy for eye therapy of 70 MeV, the effective gap voltage of 70.89 MV is applied by six cavities within 140 gaps and with a total length of 20 m. The linac consists of three coupled CH–cavities, which include an internal triplet quadrupole lens. The two tanks in these coupled structures are RF coupled by the internal cell containing the lens. The other three cavities were uncoupled CH-cavities. The idea behind a coupled cavity is to operate two single cavities as one unit with the same amplifier and consequently shorten the total length and reduce the cost. In the case of a coupled cavity, the common wall between the two cavities will be removed and replaced with a long section that hosts the triplet quadrupoles. The main linac parameters are summarized in Table 1.

In order to keep that beam focused transversely, a total of 11 triplet quadrupoles are needed along the whole linac structure, including the one transport section of a 3 MeV (MEBT). Each of the three coupled CH cavities features two KONUS periods, one in front of the focusing quadrupole triplet and the other behind the lens. The rebuncher section in the first part of the first coupled CH cavity was omitted, since the longitudinal focusing and matching are provided by the buncher at 3 MeV (in the medium beam energy transport MEBT).

The highest surplus energies are needed for the low energy section in the linac and then it is reduced gradually with increasing the particle energy. The beam parameters for the linac design are summarized in Table 2.

TABLE 1. The main parameters of the linac structure.

Total Length	20 m
Operating frequency	325.224 MHz
Average accelerating gradient	3.5 MV/m
Number of accelerating cavities	6
Rebunchers	1
Number of quadrupole lenses	11
Max on axis field	4.74 – 14.70 MV/m
Magnetic gradient for the quadrupoles	36.2 – 55.8 T/m
KONUS sections	9 in total
	8 rebunching
	9 zero degree
Gaps per sections	3-4 (rebunching)
	8-17 (zero degree)

TABLE 2. Beam parameters of the proton linac.

Ion beam type	Protons
Beam Current (mA)	1
Input/output normalized rms transverse emittance (mm mrad)	0.29/0.34
Input/output normalized rms longitudinal emittance (keV ns)	2.5/4.5
Input/output energy (MeV)	3.0 / 70.0

The simulation results from the LORASR code provide information about the realistic cavity parameters, such asthe gap length, drift tube lengths and diameters, energy, and cavity total length. The effective gap voltage distribution is simulated along each cavity and it is nearly uniform within each section and has a minimum near the quadrupole in order to reduce the electric field amplitudes that penetrate into the QT. Only tank1 in the first cavity does not follow the same behavior, instead, the voltage was increased step by step in order to reduce the electric field level to protect the cavity from a high surface electric field. Figure 5 shows the effective voltage distribution and the on-axis electric field in each gap along the whole linac.

The rms- emittance growth rates along the linac are less than 20% in the transverse planes and about 90% in the longitudinal plane as shown in Fig. 6.

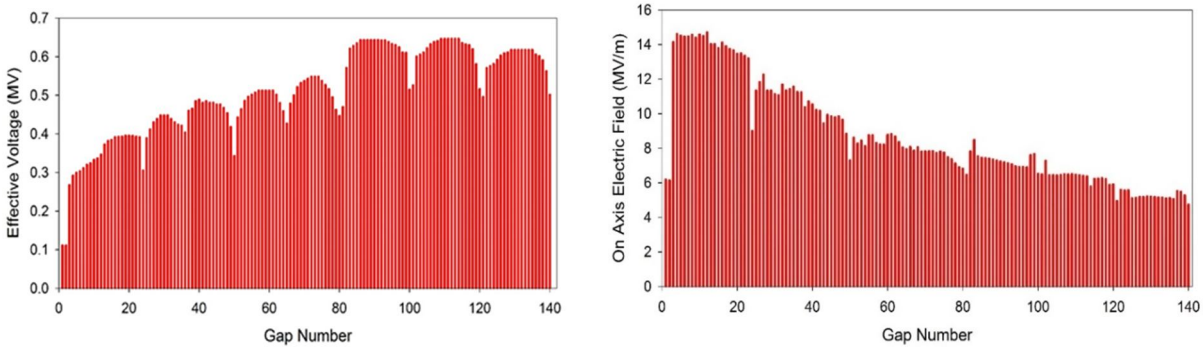

FIG. 5. Simulated effective gap voltage (left) and the on-axis electric field (right) along the whole structure. The voltage near the quadrupoles is minimized.

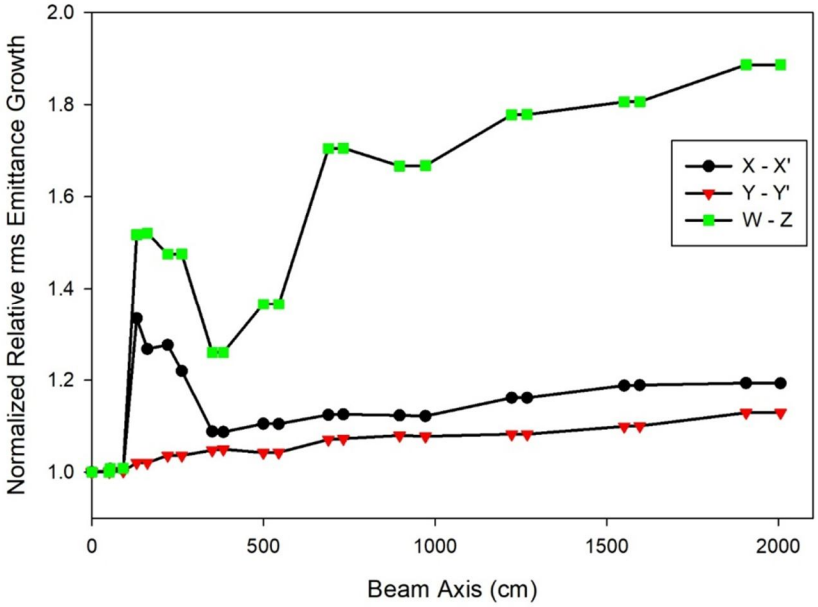

FIG. 6. Normalized relative rms-emittance growth for the matched case, where X – X' and Y – Y' are represented the transverse sub-plane and W-Z represents the longitudinal sub-plane.

The transversal and longitudinal beam envelopes (limiting lines that contain a defined percentage of the beam) are presented in Figs. 7 and 8. These two figures show the behavior of the beam in the complete 6D phase space; transversally the beam is kept narrow and its dimensions decrease significantly in the high energy side, where the risk of activation because

of potential losses becomes stronger. This should not make any problem for our design, where the beam is transported without any losses. It is important to notice from Fig. 7 how 97% of the beam needs a quadrupole aperture smaller than 10 mm, while, apart from the first lens, 99% of the beam requires around 10 mm to be transported. This information is useful in order to understand the behavior of the outer particles and to define the critical points where a potential beam loss could happen.

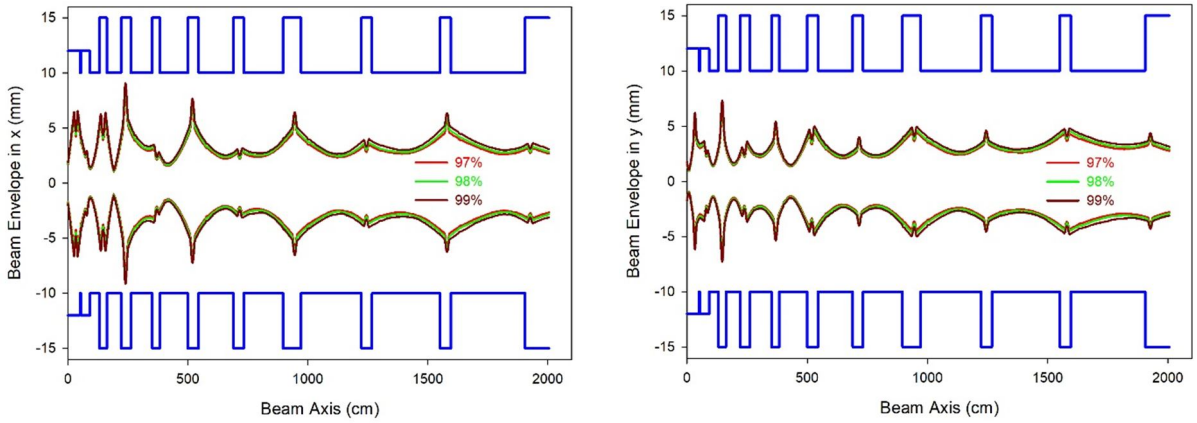

FIG. 7. A comparison between the 97%, 98%, and 99 % transversal envelope in XZ (left) and YZ plane (right).

The highest surplus energies are needed for the low-β - section of the linac. The surplus energy is reduced gradually with increasing particle velocities. Figure 8 shows the relative energy and phase envelopes in reference to the structure synchronous particle, which illustrates the KONUS periods. The stability of the longitudinal beam motion is apparent from Fig. 9, which shows the beam envelopes relative to the bunch center. The zero-degree sections of the linac are designed with surplus energies of 2%–10% at the starting phases. The energy spread is almost 1% and it will be reduced by a dedicated debuncher cavity after a long drift space. All rebuncher sections have an asynchronous phase of $\varphi_s = -35°$. The longitudinal motion of the bunch center for each zero-degree section is shown in Fig. 10.

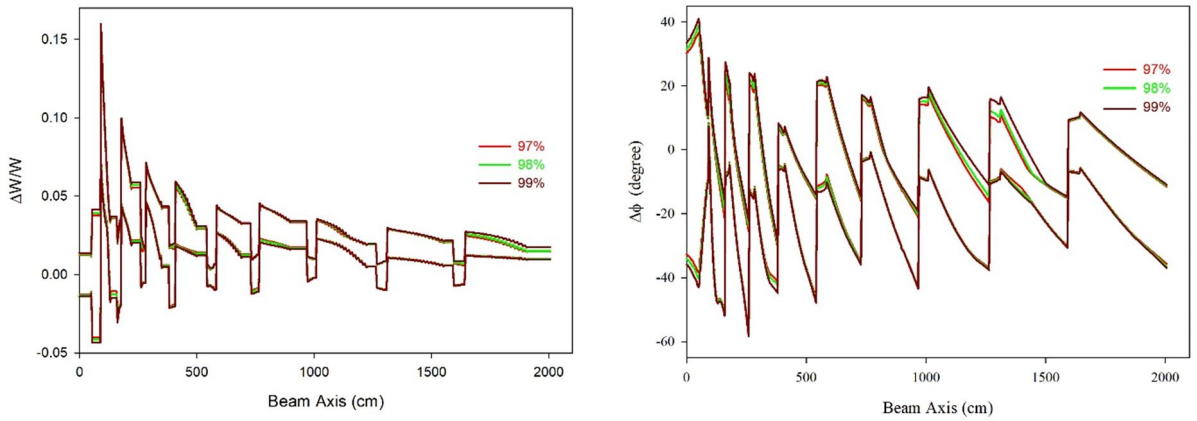

FIG. 8. Longitudinal beam envelopes along the 70 MV proton DTL. The envelopes are shown relative to the synchronous particle, as illustrated by the KONUS beam dynamics.

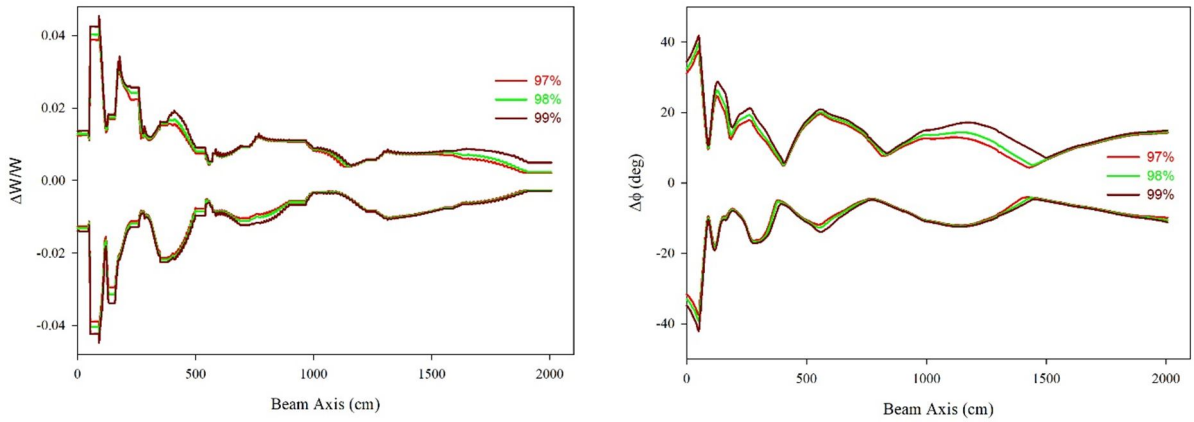

FIG. 9. Longitudinal beam envelopes along the 70 MV proton DTL, with envelopes centered around the bunch center particle.

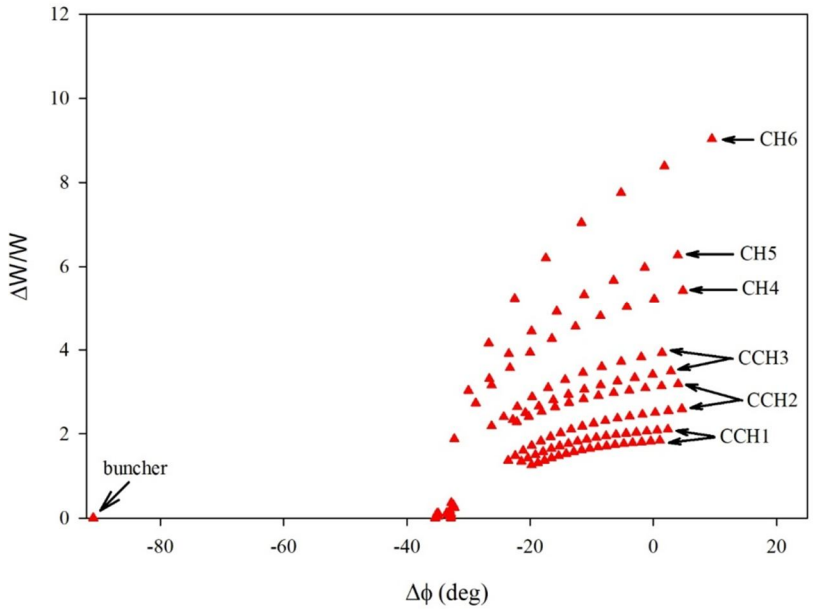

FIG. 10. The bunch center motion in the longitudinal phase space with respect to the synchronous phase.

The particle distribution at input and exit in transverse and longitudinal planes are shown in Fig. 11 for 10^6 particles. These simulations allow estimating the capability of the CH-structure for efficient beam acceleration.

The accelerated beam by this linac structure has smaller transverse beam emittances, as small as 1.8 mm mrad. This will offer a system of a pencil beam that can be moved in a transverse position to scan and cover the whole tumor volume. This can be done by using steerer or dipole magnets in order to scan the tumor cross-section. Moreover, the possibility of energy variation that can be offered by linac (see next section) will help to define the needed range of incident protons inside the tumor by adjusting the accelerator parameters. This option is not available at cyclotron where the output energy is fixed.

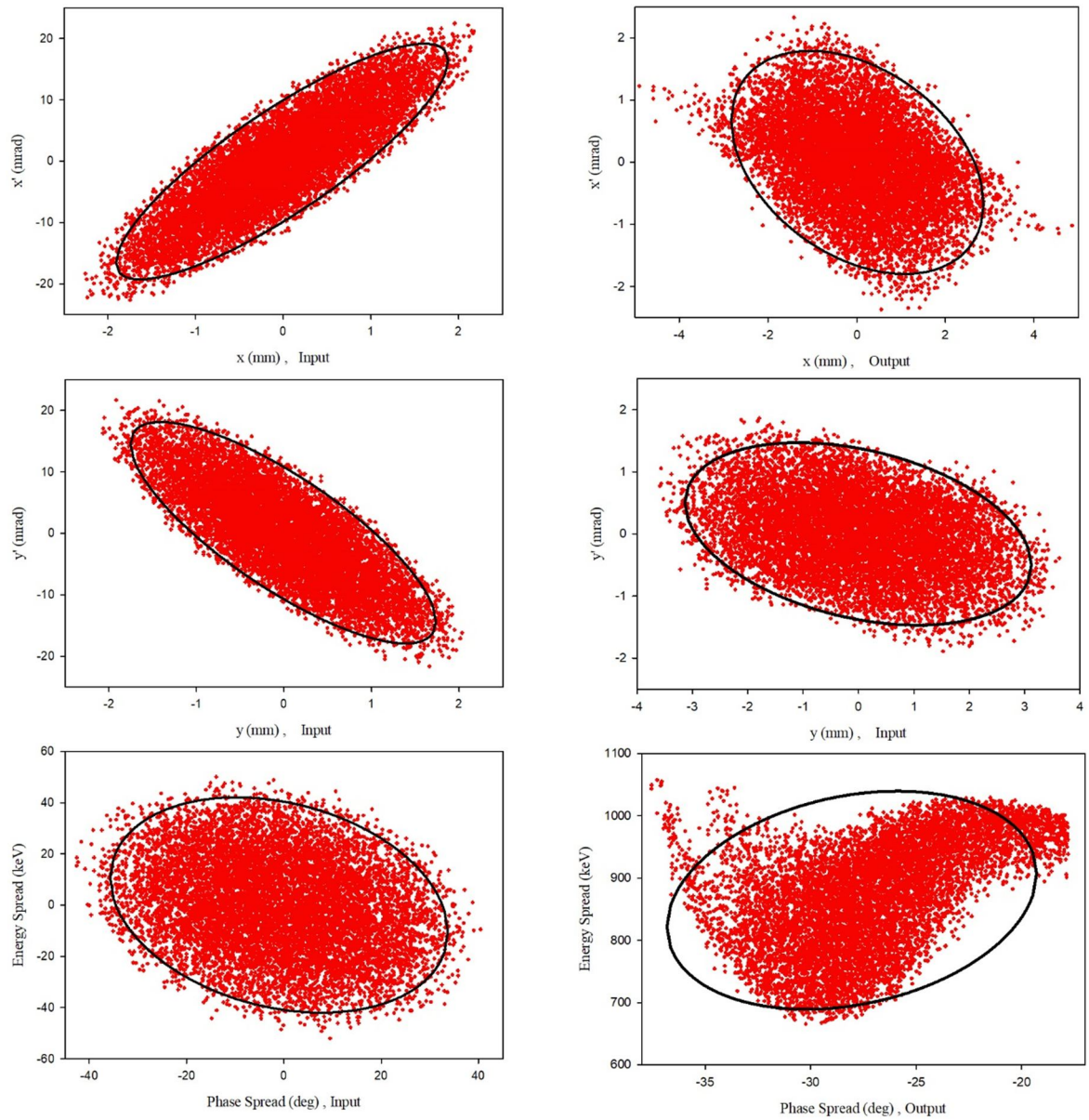

FIG. 11. Transverse (top and middle) and longitudinal (bottom) particle distribution at input and exit of the CH-DTL section at 1mA equivalent beam current. The input and output energies of the CH-DTL were 3 MeV and 70 MeV, respectively. The relevant 95% ellipses are plotted. where $x - x'$ and $y - y'$ are represented the transverse sub-plane and W-Z represents the longitudinal sub-plane.

The stability of a linac design has been investigated and the statistical error studies of the beam dynamics were performed to evaluate the tolerances for errors, such as the misalignment of components during the manufacturing and linac assembly, amplitude errors during operation, or fluctuations of beam properties. The results show that the structure is quite robust and can stand even at large error values. This includes the following: transverse displacement of the quadrupole, rotation of each quadrupole along the beamline, source error (fluctuation of input particle distribution coordinates), and cavity errors, including the voltage amplitude and phase offset. Figure 12 shows the beam transmission through the whole linac under simulated machine errors.

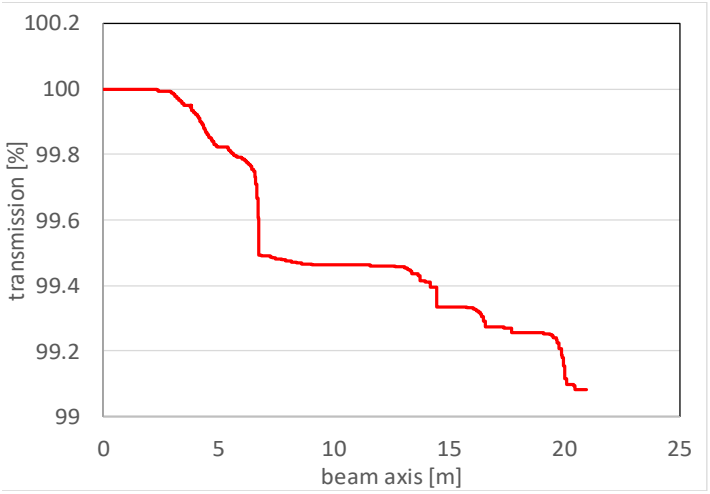

FIG. 12. The beam transmission through the while linac structure under the effect of machine error.

The additional rms emittance growth in transverse planes (x-x' and y-y') is within ±10% (95% of the runs) and in the longitudinal plane is below 50% (95% of the runs).

3.2 Energy Variation Option

As was mentioned before, many facilities have used protons with energies ranging from 58.0 to 70.0 MeV [7-15]. This option can be implemented in our design, by replacing the last cavity in our structure (Fig. 4) with two smaller tanks as shown in Fig. 13. The first tank will accelerate the protons from 58.0 MeV to about 63.3 MeV within 10 gaps, while the second tank will continue the acceleration to 70.0 MeV within 13 gaps.

The equidistant structure (EQUUS) beam dynamics [] has been used to design these two tanks. This will allow varying the proton energy smoothly by any value between 58.0–70.0 MeV by reducing the voltage of some gaps in the two tanks and drifting the proton beam until the structure ends with full beam transmission. Consequently, this will increase the beam acceptance and energy variability.

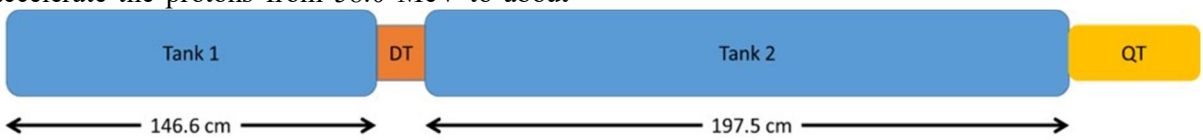

FIG. 13. The proposed structure that offers an energy variation from 58.0 - 70.0 MeV. DT and QT refer to the drift tube between the two tank cavities and triplet quadrupole, respectively.

By comparing the design of these two tanks with the cavity 6 structure in Fig. 4, both have the same length and energy range but only differ in the possibility of energy variation option.

In order to maintain efficient phase dynamics, the bunch center in the first tank starts with a negative phase of -44° and moves towards a positive phase direction. This was repeated in the second tank, where the bunch center slides back to the negative phase (-44°) and has a similar motion to that in tank 1. Fig. 14 shows the bunch center motion for both tanks.

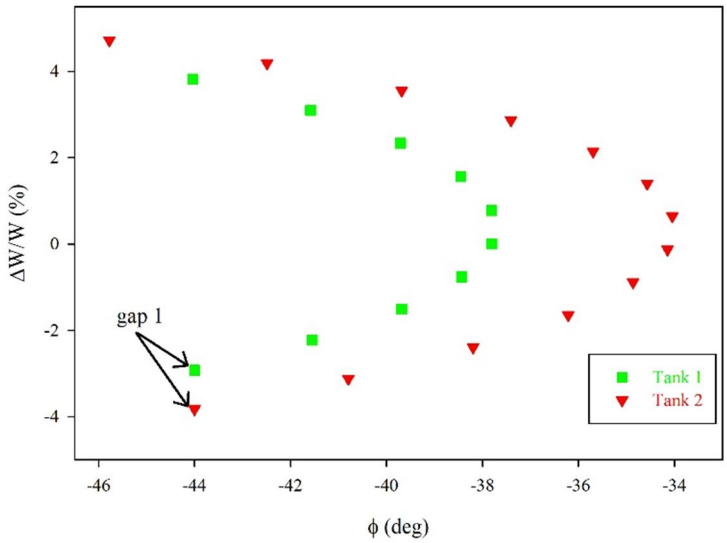

FIG. 14. The bunch center motion in the longitudinal phase space with respect to the synchronous phase.

The transversal and longitudinal beam envelopes through the two tanks are presented in Figs. 15 and 16. The beam is kept transversally narrow (smaller than 8 mm in the tanks) and requires around 8 mm within the quadrupole triplet. This is important to estimate the behavior of outer particles and to determine the possibility of beam losses.

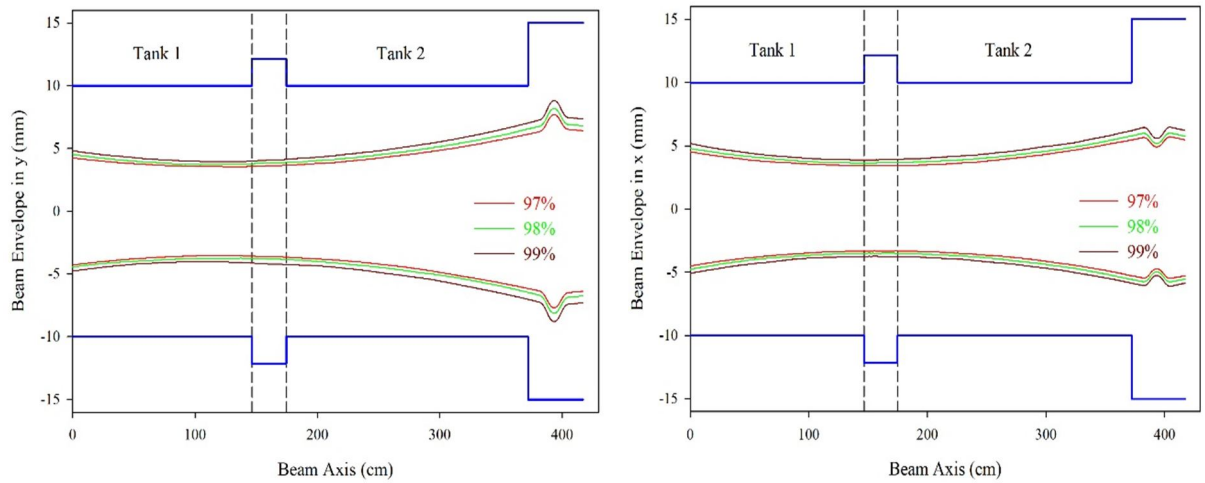

FIG. 15. A comparison between the 97%, 98%, and 99% transversal envelope in XZ (left) and YZ plane (right).

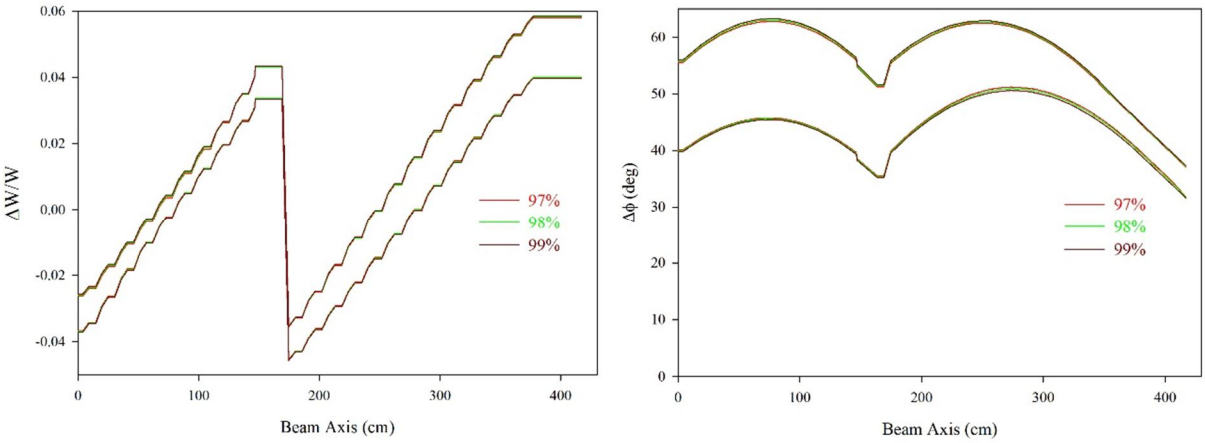

FIG. 16. Longitudinal beam envelopes along the two tanks from 58.0 to 70 MV proton energies. The envelopes are shown relative to the synchronous particle, as illustrated in the EQUUS beam dynamics.

As mentioned before, the energy variation can be realized by changing the rf voltage applied to the tank gaps. Fig. 17 shows the output energy dependence on the total applied voltage, which is not exactly a linear relation but gives a hint about the possible energy variation.

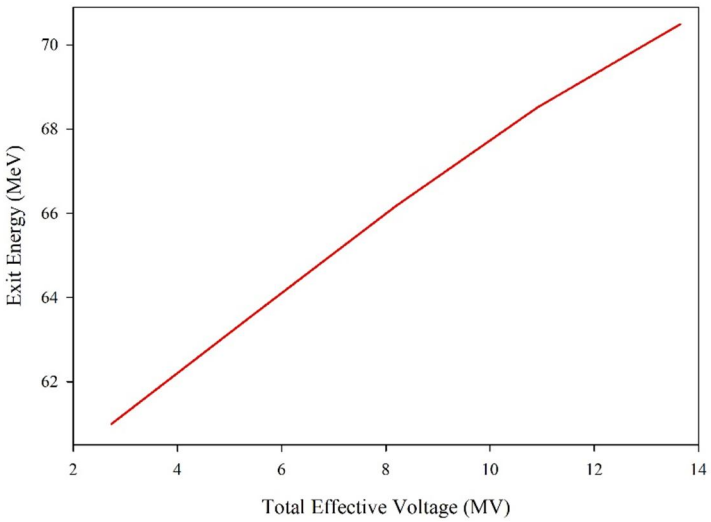

FIG. 17. Output proton energy at the end of the last two tanks in MeV versus the total applied gap voltage. This shows how the energy can be varied from 58.0 to 70.0 MeV.

4. Conclusion

The LORASR code was used to perform the KONUS beam dynamics design for a proposed DTL structure for proton eye therapy with energy ranging from 3.0 to 70 MeV. The structure consists of 6 cavities within 140 gaps and with a total length of 20 m operated at 325.224 MHz frequency. The first three cavities form a coupled structure where two CH tanks are connected by the internal cell containing a triplet quadrupole lens. The proton beam with a current of 1.0 mA was accelerated successfully through the whole structure with a transmission efficiency of 100%. The average accelerating field gradient was about 3.5 MeV/m. The optimized DTL structure has an emittance growth of less than 22% transversely and about 90% longitudinally. The transverse matching through the structure was optimized by 11 triplet quadrupoles distributed along the linac with a quadrupole aperture (diameter) of 2.4 cm in the MEBT section and 3.0 cm within and between the cavities. The maximum quadrupole field gradient attained is 94.4 T/m.

The investigation into energy variation was conducted by implementing the equidistant structure beam dynamics (EQUUS) method, which involves designing the last cavity as two tanks. The energy variation may be realized by varying the gap of voltage levels. This capability enables specialists to customize the proton beam range within the tumor based on specific requirements.

The output beam emittances are smaller than what cyclotron can offer, facilitating the generation of a pencil beam capable of scanning the tumor volume from one point to another using either a magnetic steerer or bending magnets.

It is recommended to determine the RF and mechanical model of each cavity by specifying drift tubes, gap lengths, and period lengths. Additionally, performing RF simulation using CST Studio Suite ® [26], which offers a high-performance 3D electromagnetic analysis software package for designing, analyzing, and optimizing electromagnetic (EM) components and systems, is advised. Furthermore, it is recommended to use the output particle distribution and employ simulation tools such as GENT4 or FLUKA to study the interaction between the accelerated proton beam and a simulated tumor.

References

[1] Slater, J.M., "From X-rays to Ion Beams: A Short History of Radiation Therapy". In: "Ion Beam Therapy", (Springer, Berlin, Heidelberg, 2012) pp. 3-16.

[2] Clemente, G., Ratzinger, U., Podlech, H., Groening, L., Brodhage, R. and Barth, W., Phys. Rev. Spec. Top-Ac., 14 (11) (2011) 110101.

[3] Ratzinger, U., Nucl. Meth. A, 464 (1-3) (2001) 636.

[4] Hall, E.J., Int. J. Radiat. Oncol., 65 (1) (2006) 1.

[5] Linz, U., Ed., "Ion Beam Therapy: Fundamentals, Technology, Clinical Applications". (Springer Science & Business Media, 2011).

[6] Brown, A. and Suit, H., Radiother. Oncol., 73 (3) (2004) 265.

[7] Gnacadja, E., Hernalsteens, C., Boogert, S., Flandroy, Q., Fuentes, C., Nevay, L.J., Pauly, N., Ramoisiaux, E., Shields, W., Tesse, R. and Van Roermund, R., Phys. Rev. Res., 4 (1) (2022) 013114.

[8] Swakon, J., Olko, P., Adamczyk, D., Cywicka-Jakiel, T., Dabrowska, J., Dulny, B., Grzanka, L., Horwacik, T., Kajdrowicz, T., Michalec, B. and Nowak, T., Radiat. Meas., 45 (10) (2010) 1469.

[9] Daftari, I.K., Renner, T.R., Verhey, L.J., Singh, R.P., Nyman, M., Petti, P.L. and Castro, J.R., Nucl. Instrum. Meth. A, 380 (3) (1996) 597.

[10] Cirrone, G.A.P., Cuttone, G., Lojacono, P.A., Nigro, S.L., Mongelli, V., Patti, I.V., Privitera, G., Raffaele, L., Rifuggiato, D., Sabini, M.G. and Salamone, V., IEEE T. Nucl. Sci., 51 (3) (2004) 860.

[11] Bonnett, D.E., Kacperek, A., Sheen, M.A., Goodall, R. and Saxton, T.E., Br. J. Radiol., 66 (790) (1993) 907.

[12] Herault, J., Iborra, N., Serrano, B. and Chauvel, P., Med. Phys., 32 (4) (2005) 910.

[13] Röhrich, J., Damerow, T., Hahn, W., Müller, U., Reinholz, U. and Denker, A., Rev. Sci. Instrum., 83 (2) (2012) 02B903.

[14] Blackmore, E.W., Evans, B. and Mouat, M., In Proceedings of the 1997 Particle Accelerator Conf., (Cat. No. 97CH36167) (Vol. 3, pp. 3831-3833), IEEE, (1997).

[15] Martinetti, F., Donadille, L., Delacroix, S., Nauraye, C., De Oliveira, A., Herault, J. and Clairand, I., Nucl. Technol., 168 (3) (2009) 721.

[16] Amaldi, U., Bonomi, R., Braccini, S., Crescenti, M., Degiovanni, A., Garlasché, M., Garonna, A., Magrin, G., Mellace, C., Pearce, P., Pittà, G., Puggioni, P., Rosso, E., Verdu Andrés, S., Wegner, R., Weiss, M. and Zennaro, R., Nucl. Instr. Meth. Phys. Res. A, 620 (2010) 563.

[17] Garonna, A., PhD Thesis, Swiss Federal Institute of Technology Lausanne, (2011).

[18] Ratzinger, U., Hähnel, H., Tiede, R., Kaiser, J. and Almomani, A., Phys, Rev. Accel. Beams, 22 (11) (2019) 114801.

[19] Tiede, R., Sauer, A.C., Podlech, H., Minaev, S., Ratzinger, U. and Clemente, G., LORASR code development (No. CARE-Conf-2006-006-HIPPI), (2006).

[20] Pasini, M., Calatroni, S., Delruelle, N., Lindroos, M., Parma, V. and Trilhe, P., "A SC upgrade for the REX-ISOLDE accelerator at CERN", (Energy (MeV/u), 8, 2008) p.10.

[21] Schwarz, M., Aulenbacher, K., Barth, W., Basten, M., Busch, M., Dziuba, F., Gettmann, V., Heilmann, M., Kuerzeder, T., Miski-Oglu, M. and Podlech, H., J. Phys. Conf. Ser., 1067 (5) (2018) 052006.

[22] Winkelmann, T., Cee, R., Haberer, T., Naas, B., Peters, A. and Scheloske, S., "Experience at the ion beam therapy center (HIT) with 2 years of continuous ECR ion source operation". (ECRIS08, Chicago, IL USA, MOPO-10, 2008).

[23] Tiede, R., Mäder, D., Petry, N., Podlech, H., Ratzinger, U. and Zhang, C., "Improvements of the LORASR code and their impact on current beam dynamics designs". (TUPP063, LINAC, 14, 2014).

[24] Lee, Y., Kim, E.S., Li, Z. and Hahn, G., Nucl. Instrum. Meth. A, 801 (2015) 51.

[25] Tiede, R., Ratzinger, U., Podlech, H., Zhang, C. and Clemente, G., Proc., HB'08 (2008) 223.

[26] Cst Studio Suite. https://www.3ds.com.